THE ASTROPHYSICAL JOURNAL, 475:749–759, 1997 January 10
© 1997. The American Astronomical Society. All rights reserved. Printed in U.S.A.

A DOUBLE OUTFLOW FROM A DEEPLY EMBEDDED SOURCE IN CEPHEUS

E. F. LADD
Five College Radio Astronomy Observatory, University of Massachusetts,
619 Lederle Graduate Research Center, Amherst, MA 01003

AND

K.-W. HODAPP
Institute for Astronomy, University of Hawaii, 2680 Woodlawn Drive, Honolulu, HI 96822
Received 1996 June 3; accepted 1996 August 6

ABSTRACT

We report near-infrared and submillimeter line and continuum measurements toward the embedded source IRAS 23011+6126 in the Cepheus E molecular cloud. The source has a luminosity of $70 \pm 10\ L_\odot$ and is not detected in the 2 μm continuum. Its spectral energy distribution is characterized by a very low bolometric temperature ($T_{bol} = 60$ K), placing it in the class 0 category. The source is associated with a relatively compact (0.18 pc) molecular cloud core with a mass of $8\ M_\odot$. Also associated with this source are four lobes of outflowing molecular gas. These lobes can easily be grouped into two well-collimated bipolar outflow structures with position angles differing by 52°. The small-scale outflow structure is associated with strong line emission from vibrationally excited molecular hydrogen with line ratios consistent with C shocks, while the large-scale outflow structure shows no associated molecular hydrogen emission. If one source is responsible for both flows, then the outflow mechanism must be both temporally and angularly variable. An alternate possibility is that the observed luminosity and outflow structures are generated by two sources, separated by less than 10^4 AU on the sky. Both of these sources must be very deeply embedded, and presumably quite young.

Subject heading: ISM: clouds — ISM: individual (IRAS 23011+6126) — ISM: jets and outflows

1. INTRODUCTION

The earliest phases of star formation are extremely difficult to observe, mainly because stars form deep within dusty dense cores, where the line-of-sight visual extinction may exceed 1000 mag. Most often, these sources are first detected in the far-infrared or submillimeter continuum, long before they are optically visible and often before they can be detected in the near-infrared continuum. Alternatively, these sources can also be detected via the collimated bipolar outflows they generate. Statistical analyses of outflow frequency indicate that outflows are ubiquitous among forming stars (Myers et al. 1988; Parker, Padman, & Scott 1991) and that they are present even during the very earliest phases of the star formation process (e.g., André et al. 1990; Lada & Fich 1996).

Outflows are typically detected kinematically or through the shocks they produce in ambient circumstellar material. Because of the high-velocity resolution afforded by radio-frequency observations, and the relatively high abundance of carbon monoxide in molecular clouds, searches for CO emission at velocities displaced from the ambient cloud velocity have proved quite effective in identifying bipolar flows (e.g., Snell, Loren, & Plambeck 1980; Bally & Lada 1983; Margulis, Lada, & Snell 1988; Fukui 1989). Outflows can also be mapped through observations of the shock-excited vibrational transitions of molecular hydrogen. Emission from the 2.12 μm $S(1)$ line of molecular hydrogen can be excited by relatively low-velocity (20–35 km s^{-1}) shocks, and images of its spatial distribution can often be used to delineate the structure and extent of an outflow (e.g., Davis & Eisloffel 1995; Hodapp & Ladd 1995). While the velocity resolution of these near-infrared observations cannot match that of the radio observations, the high spatial resolution and the ability to image large fields of view quickly make narrowband $S(1)$ line imaging an extremely useful complement to CO observations.

We present line and continuum observations of a deeply embedded outflow source in the Cepheus molecular cloud. Located at a distance of 730 pc (Crawford & Barnes 1970), and with a mass of $\sim 2 \times 10^4$ and a size of ~ 35 pc (Heyer, Carpenter, & Ladd 1996), the Cepheus cloud is a currently active site of star formation. Sargent (1977) mapped this cloud in CO at low spatial resolution and identified six regions of high antenna temperature, which she labeled Cep A–F. Cep A is a well-studied region of active star formation, containing several deeply embedded sources, and substantial outflow activity (e.g., Evans et al. 1981); Cep B is closely associated with the S155 H II region and also harbors forming stars (Felli et al. 1978; Panagia & Thum 1981; Minchin, Ward-Thompson, & White 1992). The other hot spots are associated with currently active, but less substantial, star formation. We present here observations of Cep E, which is associated with IRAS 23011+6126. IRAS 23011+6126 was detected as an infrared point source by the *Infrared Astronomical Satellite* (*IRAS*) with an infrared luminosity of $\sim 50\ L_\odot$. H_2O maser emission (Wouterloot & Walmsley 1986) and thermal NH_3 emission (Wouterloot, Walmsley, & Henkel 1988; Harju, Walmsley, & Wouterloot 1993) have been detected toward this source. Fukui (1989) reported detection of an outflow from this source, based on 3′ resolution CO observations, although maps were never published. This source was included in the 2.1 μm continuum survey of Hodapp (1994), who found a bipolar nebula centered on IRAS 23011+6126, and with size $\sim 40''$.

The present work began as follow-up observations in the submillimeter continuum and in CO and H_2 lines toward this source in order to characterize both the embedded source and the apparent outflow seen in the near-infrared

continuum. To our surprise, we found evidence for *two* separate outflow structures emanating from IRAS 23011+6126. In the work that follows, we discuss the implications of detecting two outflows from this very deeply embedded, and presumably quite young, source. In § 2, we describe our observations, and in § 3 we derive physical parameters from our data. In § 4, we explore plausible hypotheses for driving the observed outflow structures with one, or possibly two, young stars. We present our conclusions in § 5.

2. OBSERVATIONS AND DATA REDUCTION

We observed IRAS 23011+6126 in the 800 μm continuum and in the $J = 2 \rightarrow 1$ transitions of $C^{18}O$ and ^{12}CO during one 8 hr shift at the James Clerk Maxwell Telescope (JCMT)[1] on 1995 September 27. The 800 μm observations were repeated on the following day. In total, six continuum maps were obtained using the facility UKT-14 bolometer system with the standard broadband 800 μm filter. We chopped in azimuth with a frequency of 7.813 Hz and with a throw of 32″. We raster-scanned in the chop direction at a rate of 4″ s^{-1}, while the data were binned in 1 s intervals. From this chopped, raster-scanned data set, we reconstructed maps using the NOD2 system as modified for use at the JCMT. The six maps were then co-added to create the final image with a field of view of approximately 2′. Pointing and flux calibration were provided by frequent observations of the secondary calibration NGC 7538 (Sandell 1994). The rms uncertainty in our absolute pointing was estimated to be 1.″4 based on five-point observations toward NGC 7538, which were conducted throughout each evening. The FWHM beam size for the observations was measured to be 13.″6, based on observations of Uranus. The rms noise level for the final product was 0.15 Jy/13.″6 beam.

The spectral-line observations were also obtained using a raster-scanning method, although without chopping the secondary. We used the facility receiver A2 and scanned the telescope in right ascension across the source at a rate of 2″ s^{-1}, while the data were binned in 5 s intervals. The "OFF" observations were obtained at the end of each scan and were subtracted from the on-source scans. Both sets of spectral-line observations were taken with the digital autocorrelator spectrometer in its highest velocity resolution mode. The channel spacing in our spectra is approximately 0.1 km s^{-1}, and while the actual resolution of the instrument is known to be variable and considerably broader than this channel spacing, it is much less than the FWHM width of even our narrowest lines. For the $C^{18}O$ observations, the OFF position was located 30′ south of our (0, 0) position. Three raster-scanned maps, each with a 2′ × 2′ field of view, were co-added to produce the final data cube. The rms noise level for the data cube is ∼0.6 K in 0.1 km s^{-1} channels. Our ^{12}CO data cover a 3′ × 3′ field of view centered on IRAS 23011+6126 with approximately half the integration time of the $C^{18}O$ observations. The OFF position for the ^{12}CO observations was located 1° south of the (0, 0) position. The rms noise level for the data cube is ∼0.8 K in 0.1 km s^{-1} channels. The pointing uncertainty for the spectral-line observations was also estimated from repeated five-point continuum observations of NGC 7538 and was found to have an rms value of 2.″3.

Observations in the $J = 1 \rightarrow 0$ transition of ^{12}CO were obtained with the Five College Radio Astronomy Observatory (FCRAO)[2] 14 m telescope on 1995 December 18. We used the QUARRY 15-element receiver array (Erickson et al. 1992) and the FAAS autocorrelator to generate a half-beam–sampled map (sampling = 25.″5) of a 255″ × 306″ region around IRAS 23011+6126 with velocity resolution of ∼0.07 km s^{-1}. The observations were taken in a position-switched mode with an OFF position located approximately 6° to the east. The FWHM beamwidth (45″) and telescope efficiency ($\eta_{fss} = 0.7$) were determined from observations of Jupiter and the Moon. The data were binned into 0.8 km s^{-1} channels to improve the signal-to-noise ratio. The rms noise level for the binned data cube is 0.2 K. An rms pointing uncertainty of less than 5″ for the FCRAO observations was determined from repeated observations of the stellar SiO maser source T Cep.

Infrared imaging observations of the region around IRAS 23011+6126 were taken for us by J. Hora on 1995 October 12 with the QUIRC infrared array camera (Hodapp et al. 1996) at the University of Hawaii 2.2 m telescope on Mauna Kea. Thirty images, each with 240 s exposure time, were taken through a narrowband filter centered on the 2.12 μm *S*(1) line of vibrationally excited molecular hydrogen. The images were co-added to produce a final map with field of view of 3′ × 3′ and a pixel scale of 0.″185 $pixel^{-1}$. Absolute registration of the infrared image was obtained from coordinates of *Hubble Space Telescope* Guide Stars, several of which are located within our 3′ × 3′ field of view.

Infrared spectroscopy was obtained using KSPEC (Hodapp et al. 1994), which was recently equipped with a 1024 × 1024 HAWAII array (Hodapp et al. 1996). The 15″ long and 1″ wide spectrograph slit was oriented in the east-west direction; its position on the object was checked and documented by the slit-viewing detector of KSPEC. The weather conditions during the observations were photometric, but a combination of bad seeing and wind shake of the telescope led to poor image quality. Spectra were obtained at a slit position centered on the emission in the southern lobe and at a position centered on the bright emission knot in the northern lobe. At each position, two spectra with 200 s exposure time were taken with the telescope moved in right ascension by a few arcseconds between the exposures. Sky exposures were taken at positions to the south and north of any detectable emission from IRAS 23011+6126. A B7V star close to the object was observed for atmospheric absorption correction.

3. RESULTS

Most of our data are summarized in Figures 1 and 2. Figure 1 contains a gray-scale image of the spatial distribution of *S*(1) line emission overlaid with contours of redshifted and blueshifted ^{12}CO $J = 2 \rightarrow 1$ emission. The outflowing material is concentrated into four lobes, two of which are spatially coincident with elongated *S*(1) emission structures. The cross at the center of the map indicates the

[1] The James Clerk Maxwell Telescope is operated by The Observatories on behalf of the Particle Physics and Astronomy Research Council of the United Kingdom, the Netherlands Organisation for Scientific Research, and the National Research Council of Canada.

[2] The Five College Radio Astronomy Observatory is operated with the support of the National Science Foundation, under grant AST 94-20159 and with the permission of the Metropolitan District Commission of Massachusetts.

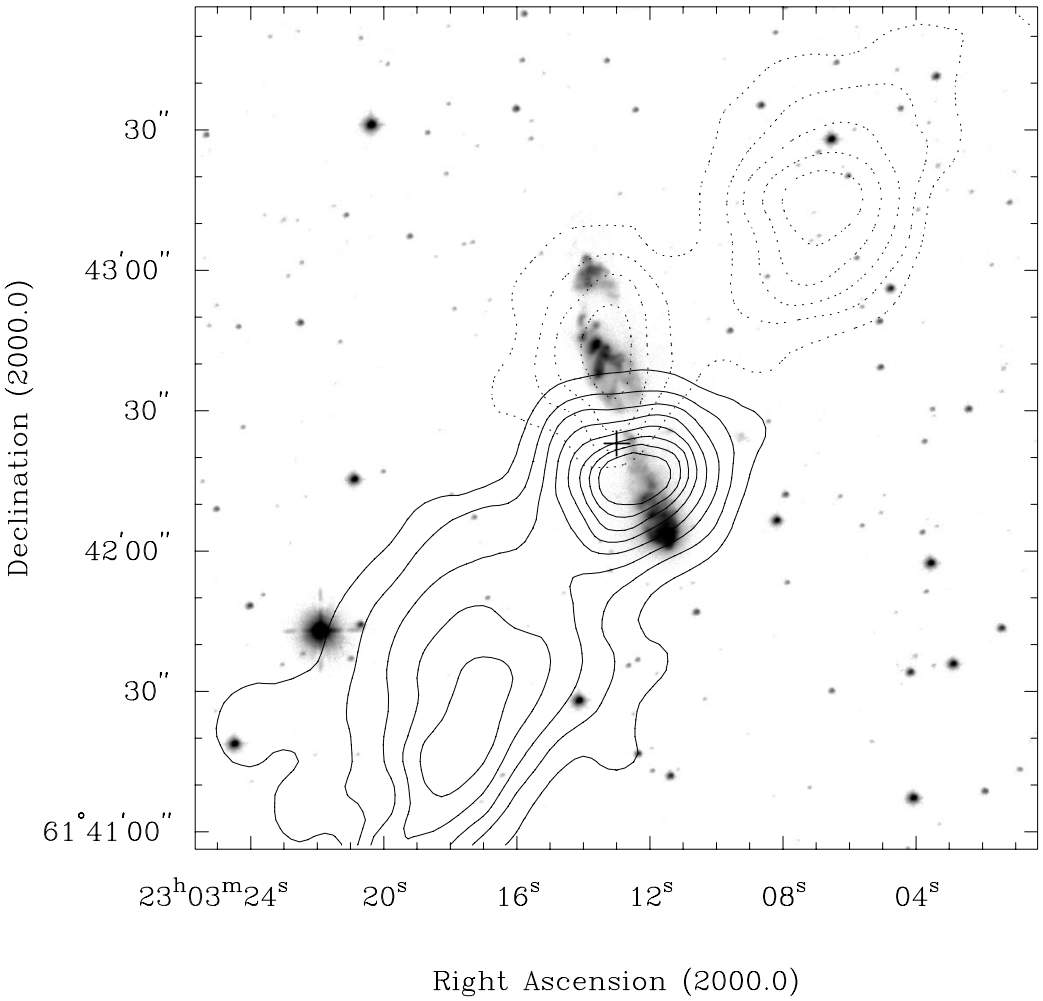


FIG. 1.—Gray scale of the 2.12 μm $S(1)$ line emission from molecular hydrogen with contours of redshifted (*dotted*) and blueshifted (*solid*) ^{12}CO $J = 2 \rightarrow 1$ emission overlaid. The blueshifted emission is the integrated intensity in the LSR velocity range -14 to -20 km s^{-1}, and the contours begin at 4 K km s^{-1} and move in increments of 4 K km s^{-1}. The redshifted emission is the integrated intensity in the LSR velocity range -6 to 0 km s^{-1}, with the same contour intervals. The systemic LSR velocity is -11.2 km s^{-1}, and the beam size of the CO observations is 21″. The cross marks the position of the 800 μm source (see Fig. 2).

position of the 800 μm source, derived from our JCMT map, which is shown in the gray scale in Figure 2. Overlaid on the gray scale in Figure 2 are contours of redshifted and blueshifted ^{12}CO $J = 1 \rightarrow 0$ emission. Although the spatial distribution of outflowing gas is quite similar to that of the $J = 2 \rightarrow 1$ emission, the division into four distinct lobes is less obvious because of the larger beam size (45″ vs. 21″) of the $J = 1 \rightarrow 0$ observations.

3.1. *Embedded Source and Surrounding Molecular Core*

The spatial distribution of 800 μm flux density was fitted with an elliptical Gaussian using the JMFIT routine in Astronomical Image Processing System. The results of this fitting procedure are summarized in Table 1. The peak flux density and integrated flux of the elliptical Gaussian fit agree well with the peak flux density and integrated flux obtained directly from the map. Combining the integrated 800 μm flux and the *IRAS* Point Source Catalog fluxes into a spectral energy distribution (SED) for the source yields a total luminosity of $70 \pm 8(1\ \sigma)\ L_{\odot}$ and a bolometric temperature $T_{\rm bol} = 61 \pm 19$ K. The bolometric temperature is comparable to those of L1527 (Chen et al. 1995), HH 24–MMS (Chini et al. 1993; Ward-Thompson et al. 1995), and L1448 N (Bachiller, André, & Cabrit 1991; Terebey, Chandler, & André 1993) and is typical of class 0 sources (Andre, Ward-Thompson, & Barsony 1993). We derive a mass based on the 800 μm total flux, and using a characteristic dust temperature of 50 K and dust opacities from Pollack et al. (1994) of 7 $M_{\odot}$. If the temperature is as low as 26 K, our mass estimate increases to 16 $M_{\odot}$.

TABLE 1

RESULTS FROM ELLIPTICAL GAUSSIAN FITTING TO 800 μm MAP

Parameter	Value
R.A. (J2000.0)	23 03 12.8
Decl. (J2000.0)	61 42 25
Major axis (arcsec)	24.4
Minor axis (arcsec)	17.8
Position angle (deg)	45
Peak flux (Jy beam^{-1})	1.31
Integrated flux (Jy)	3.1

NOTE.—Units of right ascension are hours, minutes, and seconds, and units of declination are degrees, arcminutes, and arcseconds.

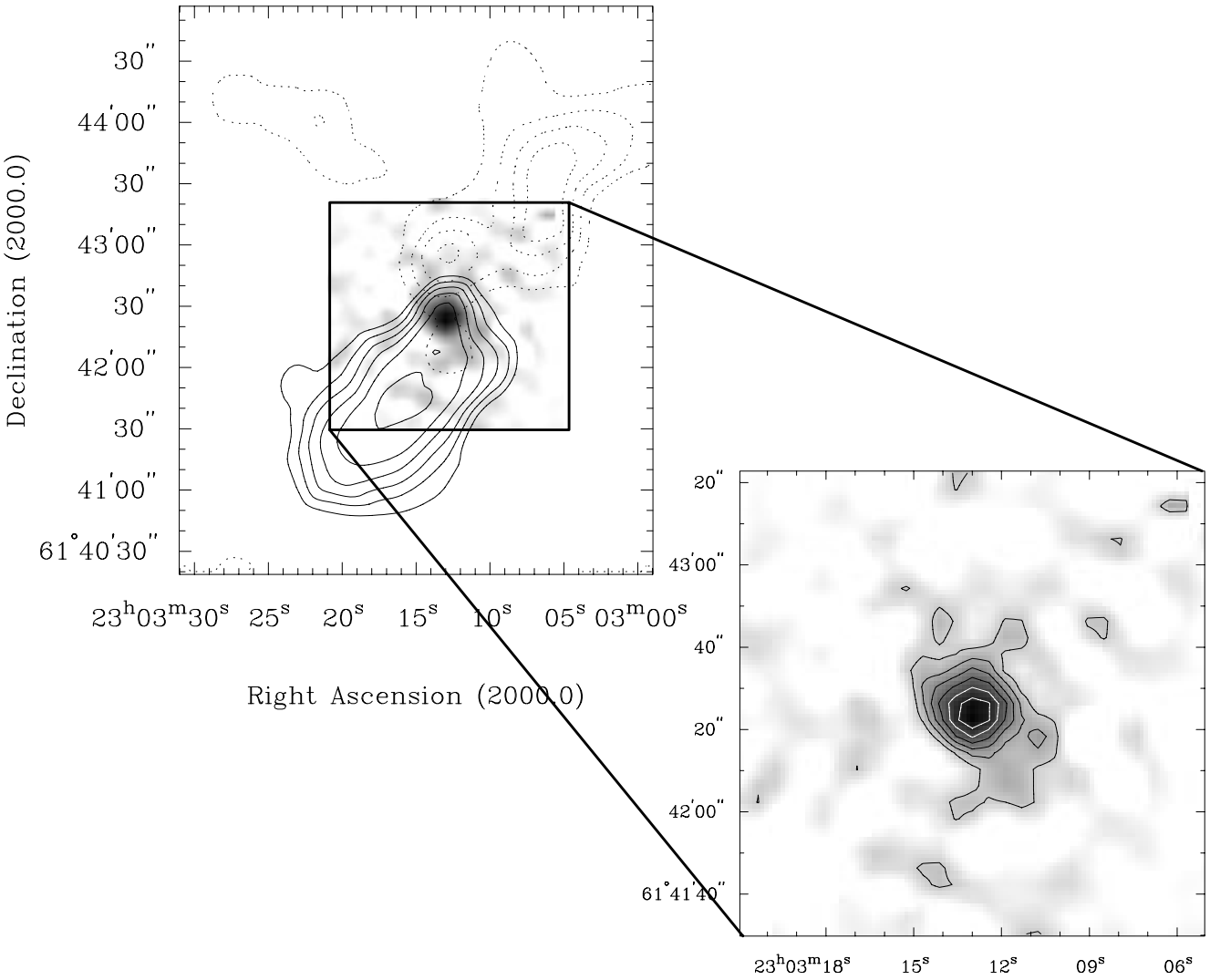


FIG. 2.—Gray-scale image of the 800 μm continuum emission from IRAS 23011+6126 with contours of redshifted (*dotted*) and blueshifted (*solid*) ^{12}CO $J = 1 \rightarrow 0$ emission overlaid. The blueshifted emission is the integrated intensity in the LSR velocity range -14 to -20 km s^{-1}, and the contours begin at 4 K km s^{-1} and move in increments of 4 K km s^{-1}. The redshifted emission is the integrated intensity in the LSR velocity range -6 to 0 km s^{-1}, with the same contour intervals. The systemic LSR velocity is -11.2 km s^{-1}. The inset shows the 800 μm continuum emission with contours that begin at 0.3 Jy beam^{-1} and move in increments of 0.2 Jy beam^{-1}. The beam size of the continuum observations is 14″, and the beam size of the CO observations is 45″.

Our C^{18}O observations delineate a dense core of FWHM size 55″. Assuming a distance of 730 pc and removing the broadening effects of the 24″ JCMT beam by subtraction in quadrature, we derive a FWHM size of 0.18 pc. For excitation temperatures ranging from 10 to 30 K, we find the C^{18}O emission is optically thin and corresponds to a peak H_2 column density of $(2.5 \pm 0.5) \times 10^{22}$ cm^{-2}. The total mass of the core, 8 $M_\odot$, and FWHM size, 0.18 pc, are comparable to the values determined by Harju et al. (1993), who derive a size of 0.18 pc and a mass of 5.8 $M_\odot$ from NH_3 observations.

3.2. *Near-Infrared Emission toward IRAS 23011+6126*

The remarkable bow tie structure seen in our $S(1)$ image was first noticed by Hodapp (1994) in a broadband K' image of this region. Our narrowband image is displayed in Figure 3, along with the results of a Lucy-Richardson deconvolution using nearby stellar images as estimates of the point-spread function. The southern portion of the bow tie has a well-defined conical shape with an opening angle of approximately 21°. The southern lobe has a very sharp southern terminus that has a classic bow-shock morphology. The northern portion has a more complicated, possibly multiple–bow-shocked morphology, but all of the strong emission is also confined within a cone of approximately 20°. Very close to the position of the submillimeter continuum source, there is a small bright knot, which Hodapp (1994) suggested could be the continuum source responsible for the apparent outflow structure.

To distinguish between H_2 emission and continuum reflection nebulosity, or thermal emission in our narrowband image, we compare the narrowband-to-broadband flux ratio for stars in the field with the same ratio for the nebulosity, using the K' image of Hodapp (1994). We find that this ratio is a factor of 6.5 ± 0.9 larger at all nebulous positions than for the average of stars in the field, while the scatter in the flux ratio for the stars was only $\approx$10%. Thus, we conclude that most of the nebulous emission is generated by transitions of vibrationally excited H_2, rather than by broadband processes such as reflection nebulosity or thermal emission. This also holds true for the emission knot near the center of the outflow and the position of the 800

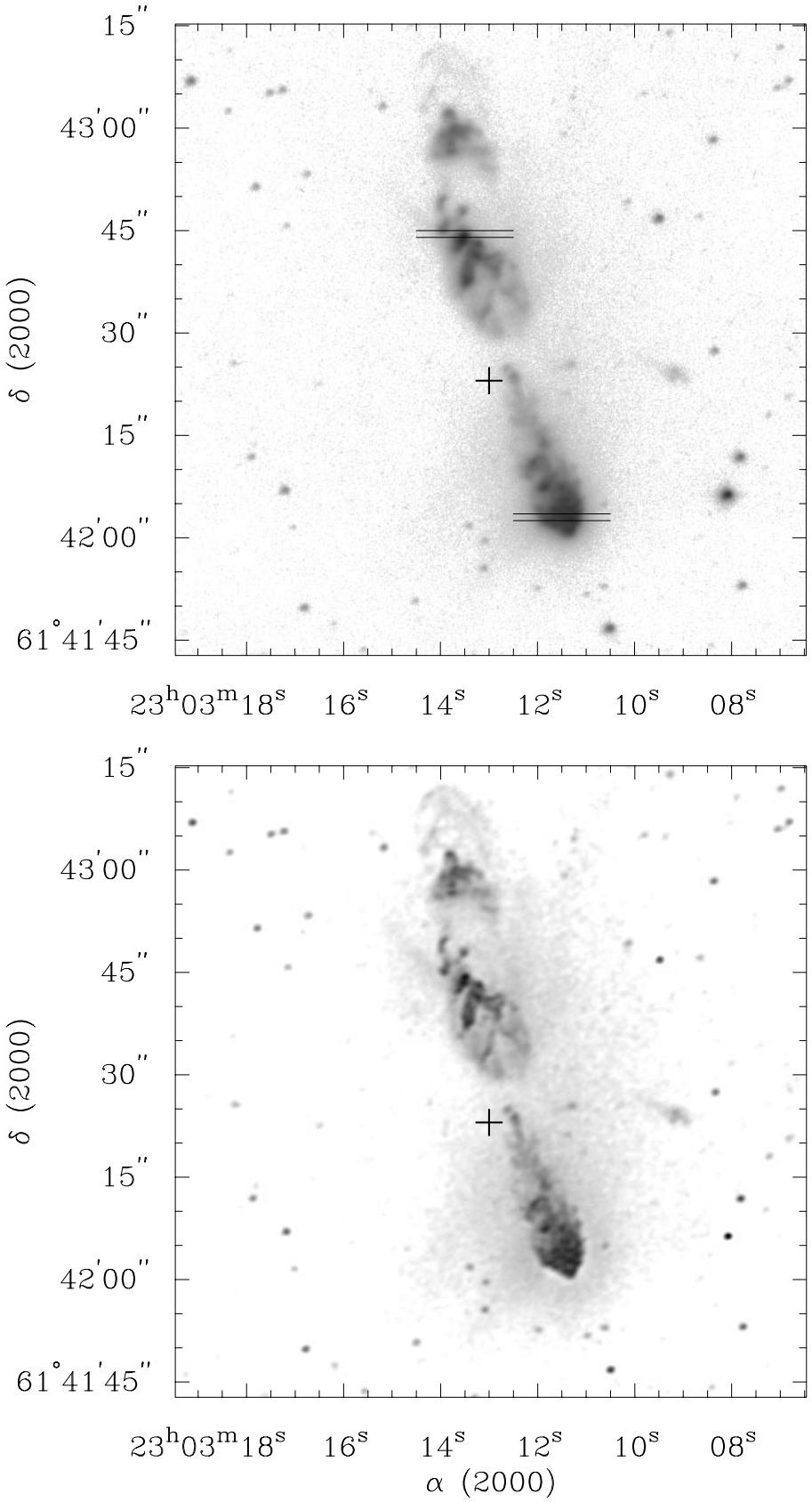


FIG. 3.—A magnified view of the *S*(1) image in Fig. 1. The positions of the KSPEC slit during the spectroscopic observations are indicated with horizontal lines. The position of the submillimeter continuum source is indicated with a cross. The bottom frame is deconvolved using 20 iterations of the Lucy-Richardson algorithm, as implemented in the IRAF STSDAS package. Both lobes show a very knotty and filamentary structure. A system of knots connects the position of the (invisible) central source with the southern lobe. Some *S*(1) emission can be seen to the west of the bipolar nebula and may be associated with the larger, older outflow.

μm source. This knot shows the same narrowband-to-broadband flux ratio as the other nebulous features.

Infrared spectra were obtained at two positions in the northern and southern lobe of the near-infrared bipolar nebula at positions indicated in Figure 3. These spectra are shown in Figure 4 in flux units, normalized to unity flux for the (1–0) $S(1)$ line at 2.12 μm. There is no detectable continuum emission in these spectra, but the molecular hydrogen lines are quite strong. The relative fluxes for other molecular hydrogen lines from the models of Smith (1995) are included in Figure 4. Smith (1995) presented two models: a J-shock model with 15 km s^{-1} shock velocity (labeled J in Fig. 4) and a C-shock model with 35 km s^{-1} velocity (labeled C here and in Fig. 4).

Our data indicate excitation levels somewhere between those two models, but the observed values are generally closer to the C-shock model than to the J shocks. In particular, higher rotational-vibrational transitions with higher excitation temperature are quite faint in our spectra. Both lobes show similar line ratios, indicating fairly similar excitation conditions.

At the position of our spectra, we do not detect continuum radiation in our spectra. These spectra, combined with the comparison between our narrowband image and the K' image from Hodapp (1994), demonstrate that the near-infrared bipolar nebula associated with IRAS 23011+6126 is almost purely molecular hydrogen emission. The similarity of the line ratios to the C-shock model implies high densities and low-ionization levels (Smith 1995) in the gas surrounding Cep E. Our nondetection of direct continuum radiation from the embedded source and the nondetection of scattered continuum radiation from the lobes both point toward an extremely deeply embedded central source for this outflow.

3.3. *Outflow*

Our ^{12}CO $J = 2 \rightarrow 1$ observations show collimated high-velocity gas extending over 36 km s^{-1} and centered on a systemic LSR velocity of -11.2 km s^{-1} derived from our C^{18}O observations. Figure 5 shows channel maps of the redshifted and blueshifted emission as a function of velocity offset from the systemic velocity. The emission is divided into four distinct lobes, best seen in the maps corresponding to velocity offsets of 10–15 km s^{-1}.

Since we have obtained both $1 \rightarrow 0$ and $2 \rightarrow 1$ observations, we can estimate the excitation temperature of the

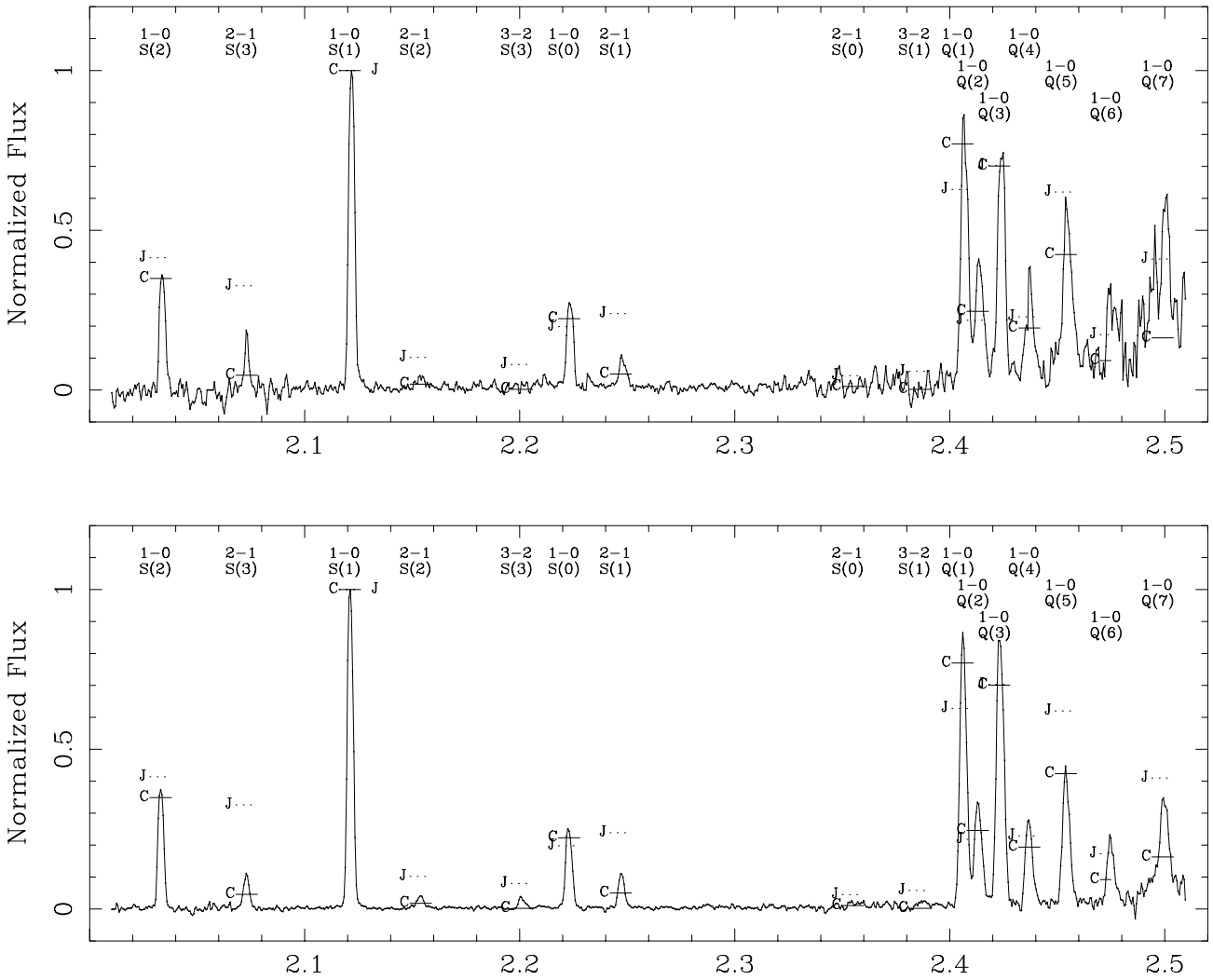


FIG. 4.—KSPEC spectra in the K window at the two positions indicated in Fig. 3. The spectra are in relative flux units, normalized for an (1–0) $S(1)$ intensity of unity. The line strengths predicted by two theoretical shock models by Smith (1995) are given for comparison. The excitation conditions in both lobes are quite similar, and both resemble the C-shock model quite well, even though the excitation seems to be somewhat higher than in that model.

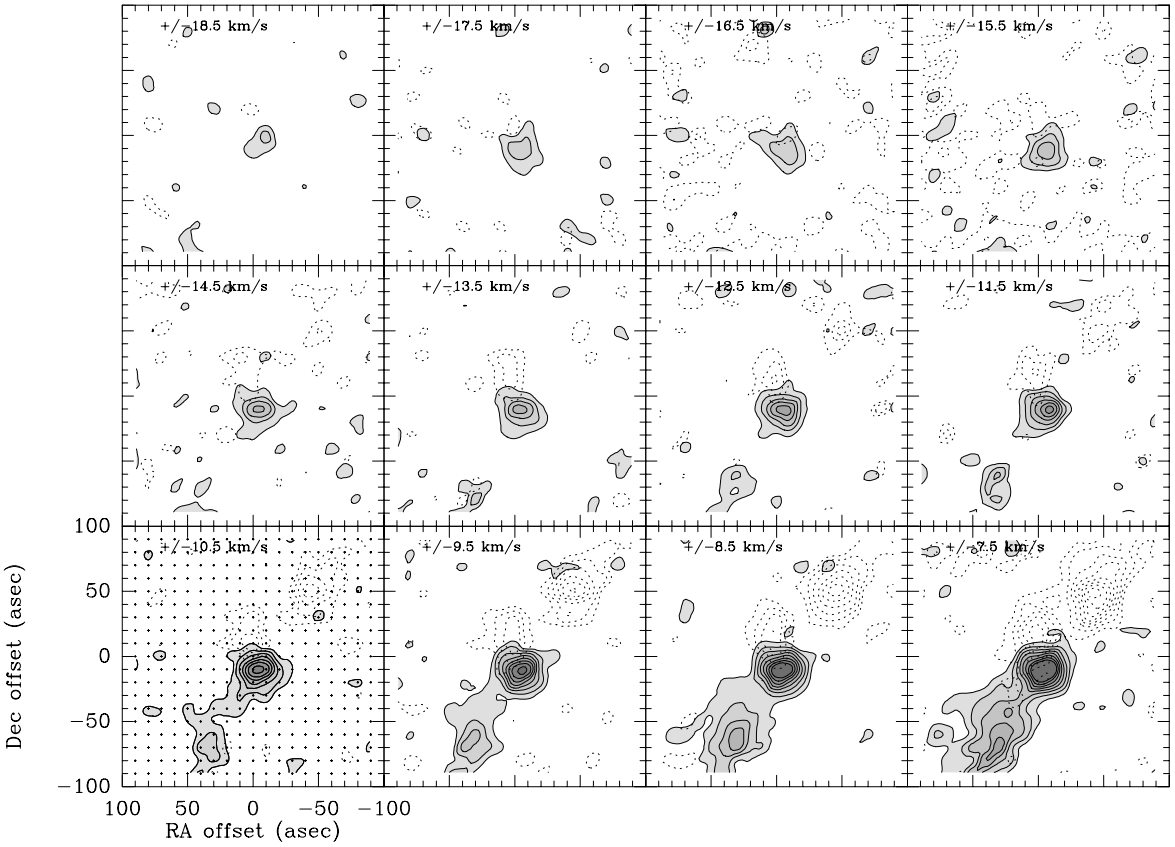


FIG. 5.—Channel maps of redshifted (*dotted contours*) and blueshifted (*solid contours with gray scale*) ^{12}CO $J = 2 \rightarrow 1$ emission toward IRAS 23011+6126. Each plot consists of the intensity integrated over a 1.0 km s^{-1} range centered on the indicated velocity. The velocities indicated in each panel are the difference between the velocity of the plotted emission and the systemic velocity.

outflowing gas. We have spatially smoothed the $2 \rightarrow 1$ data to the 45″ resolution of the $1 \rightarrow 0$ data and applied telescope efficiency corrections to both data sets.[3] At each position in the outflows, we calculated the excitation temperature from the ratio of $2 \rightarrow 1$ and $1 \rightarrow 0$ emission integrated over all outflow velocities (5–18 km s^{-1} from the systemic velocity). Over most of projected area of the outflows, we find excitation temperatures of 20 ± 5 K, although in both the red and the blue lobes there are a few positions with temperatures in excess of 30 K.[4] For the subsequent column density and mass calculations, we adopt a fixed excitation temperature of 20 K.

We have calculated the column density, mass momentum in the flow as a function of position and velocity, using both the $2 \rightarrow 1$ and the $1 \rightarrow 0$ data. For both data sets, we binned our spectra in 1 km s^{-1} bins and calculated the column density in each bin, assuming local thermodynamic equilibrium and an excitation temperature of 20 K. In all bins, the optical depth of the emission was found to be less than 1. At velocity +16 km s^{-1} from the systemic velocity (5 km s^{-1} LSR), we find emission that is not confined to the outflow lobes but appears distributed uniformly in position throughout the map; we consider this feature to be generated by a cloud component located along the line of sight, but not related to the core and outflow associated with IRAS 23011+6126, and therefore exclude this emission from our calculations. The integrated mass and momentum estimates for the redshifted and blueshifted emission are listed in Table 2. Although the mass at redshifted velocities is considerably smaller than the mass at blueshifted velocities, the momenta in the red and blue directions are quite comparable.

The division of the outflow into two redshifted and two blueshifted lobes, as well as the striking correspondence between the $S(1)$ emission and one pair of outflow lobes, leads us to conclude that two distinct outflow structures are present in our maps. The "small-scale" flow, which comprises the lobes located closest (in projection) to IRAS 23011+6126, and which is spatially associated with the $S(1)$ emission, has a position angle of 15° east of north, viewed from IRAS 23011+6126. The "large-scale" flow comprises the larger structure oriented in the northwest-southeast direction with a position angle of −37°. For purposes of calculating mass and momentum for each outflow individually, we divide the outflowing gas into small-scale and large-scale outflows separated by lines at position angle +40° and −11° measured east of north from IRAS 23011+6126. The mass and momentum for each of these outflow structures is listed in Table 2. For each outflow, the red and blue momenta are still quite comparable, although the total momentum in the large-scale flow is roughly double the momentum in the small-scale flow. The ratio of momentum to mass, which is a measure of the characteristic outflow velocity, is approximately 8 km s^{-1} for all four lobes. Using this velocity and the projected size scales of

[3] The efficiency correction for the JCMT data was determined to be 0.60, and the efficiency correction for the FCRAO data was determined to be 0.40.

[4] These higher temperatures should be regarded as only lower limits to the excitation temperature along these lines of sight, since the $2 \rightarrow 1/1 \rightarrow 0$ ratio changes little for excitation temperatures in excess of 30 K.

TABLE 2

PROPERTIES OF THE OUTFLOWING MOLECULAR GAS

Lobe	Transition	Velocity Interval (km s^{-1})[a]	Mass ($M_\odot$)	Momentum ($M_\odot$ km s^{-1})
Combined flow:				
Blue	(1–0)	2.8–14.8	0.16	0.62
	(2–1)	3.8–17.8	0.13	0.96
Red	(1–0)	5.2–15.2	0.09	0.62
	(2–1)	7.2–22.2[b]	0.08	0.78
Small-scale flow:				
Blue	(2–1)	3.8–17.8	0.03	0.24
Red	(2–1)	7.2–22.2[b]	0.02	0.17
Large-scale flow:				
Blue	(2–1)	3.8–17.8	0.06	0.40
Red	(2–1)	7.2–22.2[b]	0.04	0.44

[a] Velocity ranges in this table as referenced to the source systemic velocity, whose LSR value is -11.2 km s^{-1}.

[b] Emission within the 15.2–17.2 km s^{-1} range was excluded because most of this emission arises from a cloud component unrelated to the outflow.

0.35 and 0.1 pc for the large-scale and small-scale flows, we find dynamical timescales of 40,000 and 12,000 yr, respectively.

4. DISCUSSION

4.1. *Extreme Youth of IRAS 23011+6126*

Although measures of the ages of embedded sources are highly uncertain, all age indicators suggest that IRAS 23011+6126 is a very young source. Based on Chen et al. 's (1995) correlation between T_{bol} and the age derived from the SED models of Kenyon, Calvet, & Hartmann (1993), we estimate an age of 5000 yr. However, the models of Kenyon et al. apply to sources with luminosities an order of magnitude lower than the luminosity of IRAS 23011+6126, so this T_{bol}-determined age probably should be viewed more as evidence that the source is very young than as an accurate estimate of the source's true age. Nonetheless, the SED of IRAS 23011+6126 is clearly that of a deeply embedded source, and based on a statistical analysis of embedded and visible young sources in the Taurus cloud, Kenyon et al. estimated that the embedded phase lasts for $\sim 10^5$ yr, so this age probably provides an upper limit to the source's age. Furthermore, the SED of IRAS 23011+6126 is consistent with the most extreme embedded sources, called class 0 sources, whose ages have been estimated to be as small as 10^4 yr (André et al. 1993).

In any event, it appears that the SED-determined age of IRAS 23011+6126 is comparable to or less than the dynamical age estimated from either of the two outflow structures; this result is remarkable because the dynamical age is generally believed to be a lower limit to the age of the outflow (see, e.g., Parker et al. 1991). However, Fuller, Ladd, & Hodapp (1996) found comparable SED- and outflow-determined ages for another deeply embedded and presumably quite young source (IRAS 04368+2557 in Lynds dark cloud 1527), and it is possible that, for the youngest outflow sources, the outflow dynamical age is an accurate estimate of a source's age.

4.2. *Nature of the Double Outflow*

Perhaps the most interesting aspect of this source is the quadruple-lobed outflow structure apparently driven from IRAS 23011+6126. The geometry is such that this structure can be readily divided into two bipolar flows. The small-scale flow is clearly delineated, not only in the CO line wing emission, but also in the spatial distribution of bright, shock-excited $S(1)$ emission. There can be no doubt that the $S(1)$ lobes, and the innermost lobes of redshifted and blueshifted CO emission, trace a small (0.1 pc) bipolar outflow. The remaining two lobes of high-velocity CO emission are not associated with $S(1)$ emission, with the possible exception of two small nebulous features west of the position of the 800 μm source, but are distributed symmetrically about IRAS 23011+6126 with a projected size scale of 0.35 pc. The similarity in size, distance from IRAS 23011+6126, and velocity structure argue strongly that these structures make up a second bipolar outflow structure centered on IRAS 23011+6126.

With two well-defined bipolar outflow structures emanating from an apparently single embedded source, questions regarding the driving mechanism naturally arise. It is now widely accepted that jets from young stellar objects possess sufficient momentum to power most observed molecular outflows, and since the momentum measured in both of these outflow structures is not unusually large, a jet-driven outflow hypothesis is reasonable. Position-velocity diagrams of the emission along the axis of each outflow structure (Fig. 6) show that both the highest velocity and the brightest emission are located toward the leading edges of the flows—a morphology that is consistent with a bow-shock model, where the jet interacts most strongly with the ambient medium at its head (e.g., Masson & Chernin 1993). The $S(1)$ emission is also very bright at the leading edges of the small-scale outflow and shows the line ratios of a C shock, thus providing corroborating evidence for the bow-shock entrainment model. However, there is some $S(1)$ emission that is distributed along the outflow axis, indicating some interaction with material along the sides of the jet as well. Such interaction throughout the conical outflow lobes might be expected in the earliest phases of a jet-driven outflow, when the lobes are still being cleared of material.

The difficulty in interpreting the outflows from this source lies not in the structure of each outflow individually, but in two well-collimated and angularly distinct outflow structures that appear to emanate from a single source. There are two plausible explanations for this multioutflow structure: (1) that one time- and angle-variable–driving source has generated both outflow structures, or (2) that this "source" actually consists of two (or more) sources,

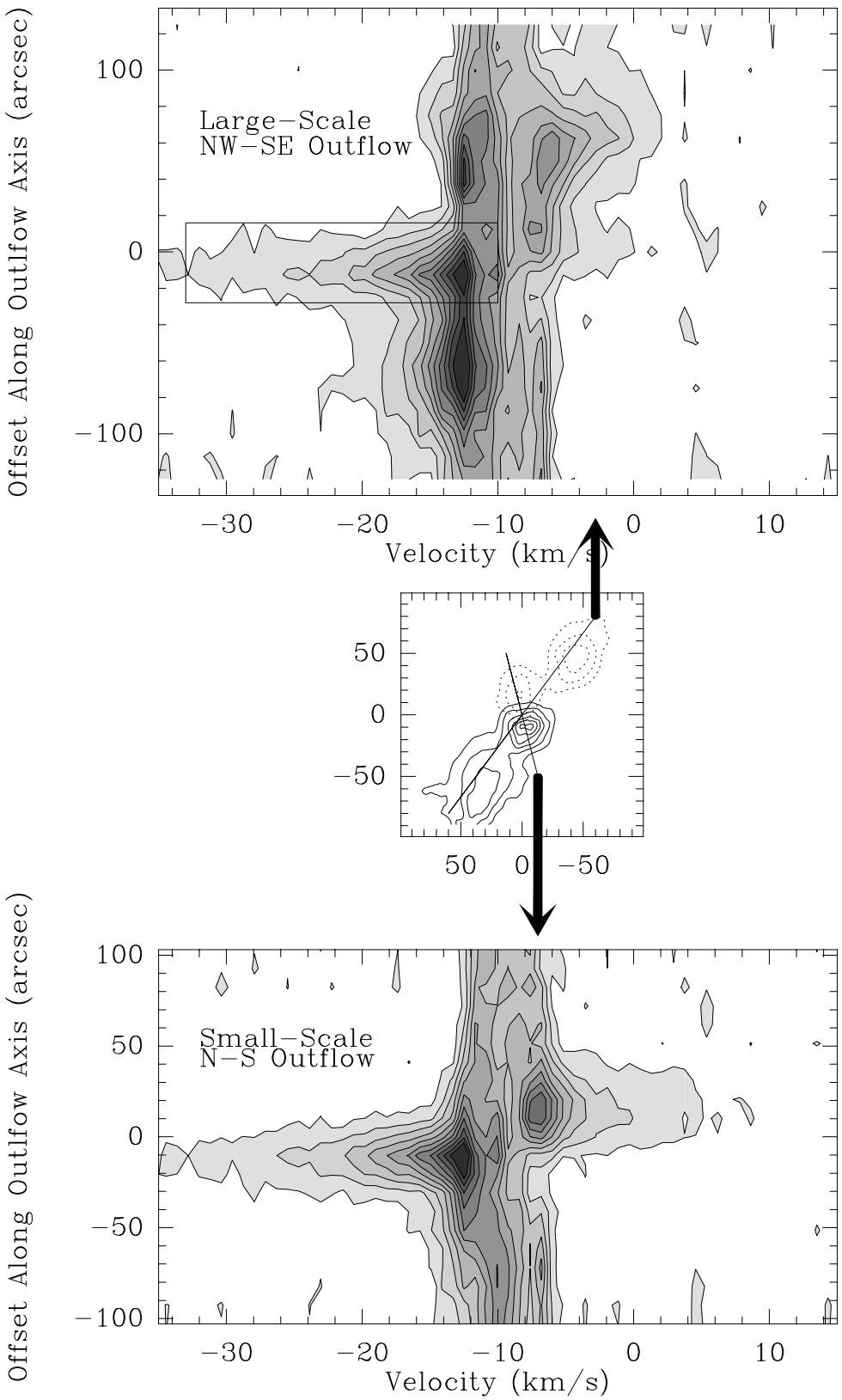


FIG. 6.—Position-velocity diagrams of the large-scale (*top*) and small-scale (*bottom*) flows. The diagram in the middle indicates the position angles of the cuts that produced the position-velocity images. The contours in both images begin at 0.5 K and move in increment of 1.0 K. Note that the blueshifted emission in the boxed area in the large-scale flow plot is part of the blue lobe of the small-scale flow.

each driving its own bipolar outflow. Next, we discuss the merits and shortcomings of each explanation.

4.2.1. *A Precessing, Time-Variable Jet?*

It is becoming more apparent that the jets driving molecular outflows are not constant in time, and probably are not constant in direction. Episodic jet activity can be inferred from the multiple–bow-shock structures seen in many $S(1)$ images of outflows [e.g., the $S(1)$ image of L1634 in Hodapp & Ladd 1995; also Davis et al. 1995], and in the spatial and velocity structure of the molecular outflows themselves (e.g., Narayanan & Walker 1996; Bachiller, Tafalla, & Cernicharo 1994). Changes in the jet angle, due to either precession or less organized "wandering," have been inferred from observations of poorly collimated molecular outflows and $S(1)$, or Hα emission that is distributed over large angles when viewed from the exciting source (Davis et al. 1995; Bence, Richer, & Padman 1996).

Thus, it is plausible to suggest that the two bipolar outflow structures emanating from IRAS 23011+6126 have been generated by one time- and angle-variable source. Indeed, the fact that only the small-scale flow currently shows $S(1)$ emission suggests that the large-scale flow might be an older, fossil flow and that only the small-scale flow is currently active. The dynamical times of the outflows support this argument also, since the large-scale flow has a dynamical time that is more than twice the dynamical time of the small-scale flow.

However, our data severely constrain this model, mainly because of the very short timescale available and the relatively large angle change required to produce both outflows. IRAS 23011+6126 has an age significantly less than 10^5 yr, probably only a few 10^4 yr. During this time, this source has generated two distinct molecular outflows whose projected position angles differ by 52°. This implies an average change in angle of the jet axis of 6×10^{-13} rad s^{-1}, a rate of change comparable to the *rotation* rates of dense cores (Goodman et al. 1993)! It is possible that the actual (i.e., three-dimensional) angular separation between the two outflow axes is less than their projected angular separation, but only if both flows are highly inclined to the line of sight. This geometry is possible, but we view it as unlikely given the high degree of collimation of the $S(1)$ emission in the small-scale outflow and the well-collimated CO emission in the large-scale flow. Even if both flows are inclined to the line of sight by 45°, their angular separation is reduced by only 20%, to 42°.

In addition to constraining the angular rate of change in the jet axis, our data also indicate that a single jet must have time-variable behavior as well. The two CO outflow structures are not blended together spatially, as might be expected of a wandering jet, but rather are distinctly separated and collimated, and there is no high-velocity emission at position angles intermediate between the two outflow axes. In addition, the two molecular hydrogen lobes are well aligned along a single axis and show no evidence of the curvature one might expect from a wandering jet. Thus, if one jet is responsible for driving both outflows, it has issued "bullets" of emission at two different position angles, and the analogy of a "loose cannon" is more appropriate than that of a "wandering fire hose."

4.2.2. *A Young Multiple System?*

Another plausible explanation for the observed outflow structure is that more than one driving source is present within the core. In this picture, the outflow structures are unrelated and have been generated by sources that are separated by only a small angular distance on the sky. Each outflow individually then becomes a more garden-variety bipolar flow, whose properties are quite typical of outflows from young sources. The luminosity of IRAS 23011+6126 is more than twice the luminosity of L1551 IRS 5, whose outflow carries more mass and momentum, and has a larger size scale then either of the flows seen here, so it is entirely reasonable to suspect that two or more sources capable of driving outflows would have a combined luminosity of only 70 $L_\odot$.

Our 800 μm continuum map shows a source size of $24'' \times 18''$ and is resolved with our $14''$ beam. If two point sources of equal intensity are responsible for the observed emission, they can be separated by no more than $\sim 15''$ (11,000 AU), and even at $15''$ separation, we would expect to resolve them into two distinct sources. If the sources have unequal 800 μm fluxes, the separation could be greater. Another constraint to this two-source model comes from the fact that no source is detected in the 2 μm continuum; therefore, both (or all of the) sources must be very deeply embedded within the dense core, and hence probably very young. Note that, although this hypothesis requires that these sources be relatively cospatial and coeval, there is no requirement that they be a binary pair. Given that the separation between the two outflow drivers might be as large as 10^4 AU, or even larger when one considers projection effects, these sources might not be bound to one another. In fact, a binary interpretation raises new problems, since it is difficult to imagine how a close binary pair might drive outflows with very different position angles. Nonetheless, the multisource hypothesis requires that these sources form from the same dense core at nearly the same time.

There is a growing list of star-forming regions that appear to harbor more than one extremely young source. On the largest scales, Myers & Ladd (1993) showed that low-$T_{\rm bol}$ sources tend to be clustered together into a few currently active star-forming sites in the Taurus cloud. Indeed, two of the three lowest $T_{\rm bol}$ sources in Taurus, L1551 IRS 5 and L1551 NE, have a projected separation of $\sim$15,000 AU. In the Perseus cloud, Sandell et al. (1991) detected a pair of class 0 sources (IRAS 4A and 4B) with projected separation of $\sim 10^4$ AU. On smaller size scales, Fuller et al. (1996) have found two submillimeter continuum sources in the L1527 core with projected separation $\sim$3000 AU, and Lay, Carlstrom, & Hills (1995) found that the two sources detected by Sandell et al. (1991) are themselves multiple sources with projected separations less than 1000 AU.

Multiaxis outflows have been used in the past to provide evidence for the presence of multiple sources. Sandell et al. (1994) detected two molecular outflows oriented nearly perpendicular to one another emanating from the embedded source IRAS 2, and they concluded that two very young sources were likely present. Bachiller, Fuente, & Tafalla (1995) have found three distinct bipolar outflow structures associated with the apparent class 0 source IRAS 20050+2720. Hodapp & Ladd (1995) found nonaligned multilobed $S(1)$ emission from IRAS2, L1634, and IRAS 08076−3556, all of which are deeply embedded, class 0–type sources. It appears now that the presence of multiple-outflow structures is frequent in extremely young

sources, suggesting either that an outflow's intensity and direction are extremely time variable in the earliest stages of star formation or that stars commonly form simultaneously in pairs or small groups.

5. CONCLUSIONS

1. We report the results of submillimeter continuum mapping of IRAS 23011+6126. At a wavelength of 800 μm, a flux of 3.1 $\pm$ 0.7 Jy was detected. The emission is resolved and well fitted by an elliptical Gaussian model with a FWHM size 24″ × 18″ (17,000 × 13,000 AU). The shape of this source's SED suggests that it is extremely young, with an age less than 10^5 yr, and probably less than 5×10^4 yr.

2. We mapped the dense core associated with IRAS 23011+6126 in the $J = 2 \rightarrow 1$ line of $C^{18}O$, and estimate a peak column density of $(2.5 \pm 0.5) \times 10^{22}$ cm^{-2} and a mass of 8 $M_\odot$.

3. We imaged a 3′ × 3′ region centered on IRAS 23011+6126 in the near-infrared through a narrowband filter centered on the $S(1)$ line of molecular hydrogen, and we detected bright bipolar nebulosity centered on IRAS 23011+6126 and extending 30″ from the submillimeter continuum position. Comparison with broadband 2 μm imaging of the same source (Hodapp 1994) as well as spectra taken toward two positions in the nebula indicate that line emission from vibrationally excited molecular hydrogen is the dominant contributor to the observed emission.

4. The observed molecular hydrogen line ratios in the southern and northern lobes of Cep E are quite similar to those predicted from C shocks in dense gas of low ionization.

5. We searched a 4′ × 3′ region centered on IRAS 23011+6126 for high-velocity ^{12}CO $J = 1 \rightarrow 0$ emission, and a slightly smaller region for $2 \rightarrow 1$ emission. We detected four lobes of high-velocity emission, two of which exhibit redshifted velocities and two of which exhibit blueshifted velocities. The spatial distribution of the redshifted and blueshifted lobes indicates strongly that two bipolar outflows emanate from IRAS 23011+6126.

6. It is possible that one source could drive the two observed outflow structures, but this source must be rapidly variable both in time and in direction to have generated two collimated outflows with very different positions angles during its short lifetime.

7. It is also quite possible that IRAS 23011+6126 actually consists of two or more sources, and that the observed outflows are driven independently. If there are two or more sources in this region, they are constrained to be separated by no more than 10^4 AU in projection, and by no more than 4×10^4 yr in age.

We thank J. Hora for obtaining the 2.12 μm imaging data for us.

REFERENCES

André, P., Martin-Pintado, J., Despois, D., & Montmerle, T. 1990, A&A, 236, 180
André, P., Ward-Thompson, D., & Barsony, M. 1993, ApJ, 406, 122
Bachiller, R., André, P., & Cabrit, S. 1991, A&A, 241, L43
Bachiller, R., Fuente, A., & Tafalla, M. 1995, ApJ, 445, L51
Bachiller, R., Tafalla, M., & Cernicharo, J. 1994, ApJ, 425, L93
Bally, J., & Lada, C. J. 1983, ApJ, 265, 824
Bence, S. J., Richer, J. S., & Padman, R. 1996, MNRAS, 279, 866
Chen, H., Myers, P. C., Ladd, E. F., & Wood, D. O. S. 1995, ApJ, 455, 377
Chini, R., Krugel, E., Haslam, C. G. T., Kreysa, E., Lemke, R., Reipurth, B., Sievers, A., & Ward-Thompson, D. 1993, A&A, 272, L5
Crawford, D. L., & Barnes, J. B. 1970, AJ, 75, 692
Davis, C. J., & Eisloffel, J. 1995, A&A, 300, 851
Davis, C. J., Mundt, R., Eisloffel, J., & Ray, T. P. 1995, AJ, 110, 766
Erickson, N. R., Goldsmith, P. F., Novak, G., Grosslein, R. M., Viscuso, P. J., Erickson, R. B., & Predmore, C. R. 1992, IEEE Trans. on Microwave Theory and Techniques, 40, 1
Evans, N. J., et al. 1981, ApJ, 244, 115
Felli, M., Tofani, G., Harten, R. H., & Panagia, N. 1978, A&A, 69, 199
Fukui, Y. 1989, in ESO Conf. Proc. 33, Workshop on Low-Mass Star Formation and Pre–Main-Sequence Objects, ed. B. Reipurth (Garching: ESO), 2
Fuller, G. A., Ladd, E. F., & Hodapp, K.-W. 1996, ApJ, 463, L97
Goodman, A. A., Benson, P. J., Fuller, G. A., & Myers, P. C. 1993, ApJ, 406, 528
Harju, J., Walmsley, C. M., & Wouterloot, J. G. A. 1993, A&AS, 98, 51
Heyer, M. H., Carpenter, J. M., & Ladd, E. F. 1996, ApJ, 463, 630
Hodapp, K.-W. 1994, ApJS, 94, 615
Hodapp, K.-W., Hora, J. L., Irwin, E., & Young, T. 1994, PASP, 106, 87
Hodapp, K.-W., et al. 1996, NewA, submitted
Hodapp, K.-W., & Ladd, E. F. 1995, ApJ, 453, 715
Kenyon, S. J., Calvet, N., & Hartmann, L. 1993, ApJ, 414, 676
Lada, C. J., & Fich, M. 1996, ApJ, 459, 638
Lay, O. P., Carlstrom, J. E., & Hills, R. E. 1995, ApJ, 452, L73
Margulis, M., Lada, C. J., & Snell, R. L. 1988, ApJ, 333, 316
Masson, C. R., & Chernin, L. 1993, ApJ, 414, 230
Minchin, N. R., Ward-Thompson, D., & White, G. 1992, A&A, 265, 733
Myers, P. C., Heyer, M., Snell, R. L., & Goldsmith, P. F. 1988, ApJ, 324, 907
Myers, P. C., & Ladd, E. F. 1993, ApJ, 413, L47
Narayanan, G., & Walker, C. K. 1996, ApJ, 466, 844
Panagia, N., & Thum, C. 1981, A&A, 98, 295
Parker, N. D., Padman, R., & Scott, P. F. 1991, MNRAS, 252, 442
Pollack, J. B., Hollenbach, D., Beckwith, S., Simonelli, D. P., Roush, T., & Fong, W. 1994, ApJ, 421, 615
Sandell, G. 1994, MNRAS, 271, 75
Sandell, G., Aspin, C., Duncan, W. D., Russell, A. P. G., & Robson, E. I. 1991, ApJ, 376, L17
Sandell, G., Knee, L. B. G., Aspin, C., Robson, I. E., & Russell, A. P. G. 1994, A&A, 285, L1
Sargent, A. I. 1977, ApJ, 218, 736
Smith, M. D. 1995, A&A, 296, 789
Snell, R. L., Loren, R. B., & Plambeck, R. L. 1980, ApJ, 239, L17
Terebey, S., Chandler, C. J., & André, P. 1993, ApJ, 414, 759
Ward-Thompson, D., Chini, R., Krugel, E., André, P., & Bontemps, S. 1995, MNRAS, 274, 1219
Wouterloot, J. G. A., & Walmsley, C. M. 1986, A&A, 168, 237
Wouterloot, J. G. A., Walmsley, C. M., & Henkel, C. 1988, A&A, 203, 367